



City Research Online

City, University of London Institutional Repository

Citation: Ghosh, S. & Rahman, B. M. (2019). Design and optimization of compact silicon photonic sensors. Proceedings of SPIE - The International Society for Optical Engineering, 11043, doi: 10.1117/12.2502509 ISSN 0277-786X doi: 10.1117/12.2502509

This is the published version of the paper.

This version of the publication may differ from the final published version.

Permanent repository link: <https://openaccess.city.ac.uk/id/eprint/21830/>

Link to published version: <https://doi.org/10.1117/12.2502509>

Copyright: City Research Online aims to make research outputs of City, University of London available to a wider audience. Copyright and Moral Rights remain with the author(s) and/or copyright holders. URLs from City Research Online may be freely distributed and linked to.

Reuse: Copies of full items can be used for personal research or study, educational, or not-for-profit purposes without prior permission or charge. Provided that the authors, title and full bibliographic details are credited, a hyperlink and/or URL is given for the original metadata page and the content is not changed in any way.

City Research Online:

<http://openaccess.city.ac.uk/>

publications@city.ac.uk

PROCEEDINGS OF SPIE

SPIDigitalLibrary.org/conference-proceedings-of-spie

Design and optimization of compact silicon photonic sensors

Souvik Ghosh , B. M. A. Rahman

Souvik Ghosh , B. M. A. Rahman, "Design and optimization of compact silicon photonic sensors," Proc. SPIE 11043, Fifth Conference on Sensors, MEMS, and Electro-Optic Systems, 110430N (24 January 2019); doi: 10.1117/12.2502509

SPIE.

Event: Fifth Conference on Sensors, MEMS, and Electro-Optic Systems, 2018, Skukuza, South Africa

Design and optimization of compact silicon photonic sensors

Souvik Ghosh^a and B. M. A. Rahman^a

^aCity, University of London, Northampton Square, London EC1V 0HB, UK

ABSTRACT

Although optical sensors incorporating grating inscribed and etched fibres are now sufficiently mature and well established in the market, however, designs based on more exotic nanowires and photonic crystal fibres are becoming increasingly important and showing much improved sensitivity by accessing a larger evanescent field. Similarly, novel planar design concepts, such as the silicon slot guide-based design is showing even greater promise, allowing the exploitation of well-developed CMOS fabrication technologies for potentially low-cost sensor elements. In compact Integrated Optic format, dielectric slots, plasmonic slots, Mach-Zehnder interferometer, and ring resonators are also emerging as novel photonic sensors. However, high index contrast also makes the modes in such sensing structures fully hybrid in nature and in such a case, full-vectorial rigorous numerical approaches will be necessary for their design optimization. Some selected results for silicon based compact photonic sensors will be presented illustrating the value and potential of the computationally efficient finite element method in such designs.

Keywords: Silicon-on-insulator (SOI), Finite element method, Slot waveguide, Sensors

1. INTRODUCTION

The development of slot waveguides has created new opportunities for exotic optical sensor by guiding light in low index sensing area, such as air or water in the slot region and thus creating the potential for more advanced, sensitive yet very compact and low-cost photonic sensors. The design and optimization of such novel vertical slots,¹ horizontal slots² and polarization independent cross-slots³ for biosensing will be presented. The design of a novel plasmonic slot supporting complex plasmonic modes for gas sensing⁴ will also be presented. The design optimization of metal coated silica nanowire for bio sensing⁵ and doped ZnO coated gold nanowire⁶ for gas sensing and a resonating straight slots⁷ for biosensing will also be presented. All these devices and waveguides were simulated by and their sensing responses were investigated with our in-house full-vectorial finite element method. Over last thirty years we modified our code for different types of low and high-index contrast devices. Even lossy plasmonic waveguides and complex hybrid and composite plasmonic waveguides have been analyzed with our versatile and accurate method. In this article we will limit our discussion to the applications of finite element based modal solution for designing nano level photonic devices.

2. FULL-VECTORIAL FINITE ELEMENT METHOD (FV-FEM)

A vector variational formulation has been developed to analyze the electromagnetic wave propagation through dielectric and metallic waveguides. The necessity of the vector formulation was realized when the scalar formulation showed its inefficiency because of the presence of inhomogeneous or anisotropic media. The full-vectorial formulation solves a wide range of the waveguides with complex shapes, sizes, and material compositions. To setup the FV-FEM method, the entire cross-section of the of interest is subdivided into small triangular sub-domains, also called elements. These small elements may have different shapes depending on the waveguide cross-section. However, triangular elements are the best fit for any complex structure with straight and slanted material boundaries. Although, for circular optical fiber we developed spherical coordinate meshing technique which provides much better result compare to the Cartesian coordinate based triangular mesh distribution. After meshing, the electromagnetic field functions are defined by a set of polynomials over each mesh element. Finally, a variational functional is then minimized with respect to the field components at the vertices of the

Further author information: (Send correspondence to B. M. A. Rahman)
B. M. A. Rahman: E-mail: b.m.a.rahman@city.ac.uk

Fifth Conference on Sensors, MEMS, and Electro-Optic Systems, edited by Monuko du Plessis,
Proc. of SPIE Vol. 11043, 110430N · © 2019 SPIE · CCC code: 0277-786X/19/\$18 · doi: 10.1117/12.2502509

elements. These element vertices also referred as nodes. A benefit of such subdivision is that the distribution of the unknown field is also discretized into subzones. Now the subdivided elements are easy to examine to find out the localized distribution of the unknown field components compared to the inspection of entire domain.

In 1956, Berk⁸ proposed several electromagnetic field based approaches such as **H**-field, **E**-field, **E**+**H**-field, and E_z+H_z -field to formulate those electromagnetic fields into a variational form. Among them, the **H**-field based formulation is simple and accurate compared to others. In this article we used the **H**-field based formulation to model our proposed photonic sensors. Applying the minimum theorem, the variational of the functional **F** based on Maxwell's curl equations must be zero i.e. $\delta\mathbf{F} = 0$. The function F can be expressed as

$$\mathbf{F} = \langle \hat{\epsilon}_r^{-1} (\nabla \times \mathbf{H}), (\nabla \times \mathbf{H}) \rangle - \omega^2 \langle \hat{\mu} \mathbf{H}, \mathbf{H} \rangle \quad (1)$$

Here the parameters ω , $\hat{\epsilon}$, and $\hat{\mu}$ are the angular frequency, permittivity and permeability tensors, respectively. The braces in Eq. 1 indicates the inner product with the equation form of $\langle A, B \rangle = \iint B^* \cdot A \, dx dy$. The Euler form of Eq. 1 satisfy the Helmholtz's equation but unfortunately that does not satisfy Maxwell's two divergence equations. Therefore, the solution contains unwanted non-physical solutions along with the physical solutions. Rahman and Davies proposed a successful way to balance the curl and divergence part of the equation by using penalty function method where a weighting factor close to the value of $1/n_{eff}^2$ was used to balance the effect of divergence and the curl equations. The extremum eigenvalue equation from the reformed variational formulation can be expressed as

$$\omega^2 = \frac{\iint [(\nabla \times \mathbf{H})^* \cdot \hat{\epsilon}^{-1} (\nabla \times \mathbf{H}) + p (\nabla \cdot \mathbf{H})^* (\nabla \cdot \mathbf{H})] \, dx dy}{\iint \mathbf{H}^* \cdot \mu \mathbf{H} \, dx dy} \quad (2)$$

The **H** and * denote the full-vectorial magnetic field and complex conjugate transpose. These method is successful and accurate to determine the modal field distributions and propagation constants of the fundamental and higher order quasi-TE and TM modes. However, it is less effective in solving the plasmonic waveguides and a combination of dielectric and plasmonic waveguides. Recently, Souvik and Rhaman^{9,10} modified the variational formulation by considering the contributions of both positive and negative permittivities of local element material into additional divergence-divergence part of Eq. 2. Here, only a 2-D waveguide cross-section is considered for wave propagation. On the other hand, the resonator cavity needs a 3-D approach and then the variation formulation needs to be integrated over a three dimensional computational domain.⁷

3. PHOTONIC SENSING DEVICES

In the following sections we presented some of our works on on-chip photonic sensing devices using our in-house accurate numerical simulation tool.

3.1 SOI based vertical and horizontal slot waveguide

A silicon-on-insulator (SOI) based vertical slot waveguide was designed by keeping two nano dimensional silicon (Si) cores close together that simultaneously creates a small nano-gap for light guiding and confinement. A schematic cross-section of the vertical slot waveguide is shown in Fig. 1(a). In a similar manner, a horizontal slot waveguide have been formed by closing two Si slabs in vertical direction. Therefore, a nano-gap in the horizontal section confines a large fraction of light, shown in Fig. 1(b). In these waveguides, the light-wave propagates through the low index slot region and this could be explained from electromagnetic boundary conditions derivable from Maxwells equations. It demands that for a high index contrast dielectric interface, the normal component of electric flux density (**D**) must be continuous, i.e. $D_{n1} = D_{n2}$. This results in a discontinuity of the corresponding electric field (E_n). Therefore, a large fraction of the electric field (**E**) can be confined and guided by the low index slot region.

Both the vertical and horizontal slot waveguides were used to detect the DNA hybridization process. A 8 nm single stranded DNA while converted into a double stranded DNA its refractive index changes from 1.456 to 1.530. This index difference in an ultra-thin layer could be detected by both the waveguides. The waveguide design parameters were optimized for their best response. The vertical slot waveguide shows its maximum light

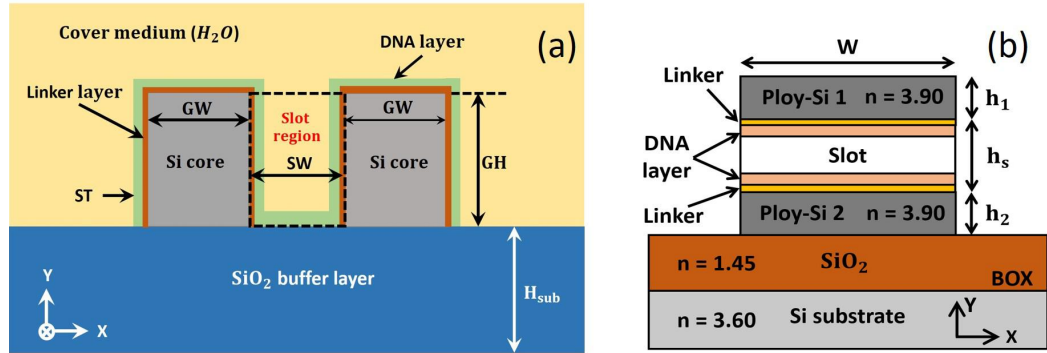


Figure 1. Artistic cross-sectional view of SOI based vertical (a) and horizontal (b) slot waveguides.

confinement for the Si core height of 320 nm. Figure 2(a) shows the variation of effective index difference (Δn_{eff}) and sensitivity with the Si core guide width for different slot widths such as SW = 60, 100, and 140 nm. The lower the SW better is the waveguide sensitivity. Similarly, Figs. 2(b) shows the n_{eff} and Δn_{eff} variations with guide width and shows a maximum Δn_{eff} for the width = 0.70 μm . Both the vertical and horizontal slot waveguides can be incorporated for ring resonator and Mach-Zehnder interferometer based sensing devices. The SOI vertical slotted ring resonator shows a 6.12 nm wavelength shift with a sensitivity of 856 nm/RIU during the detection of DNA hybridization.

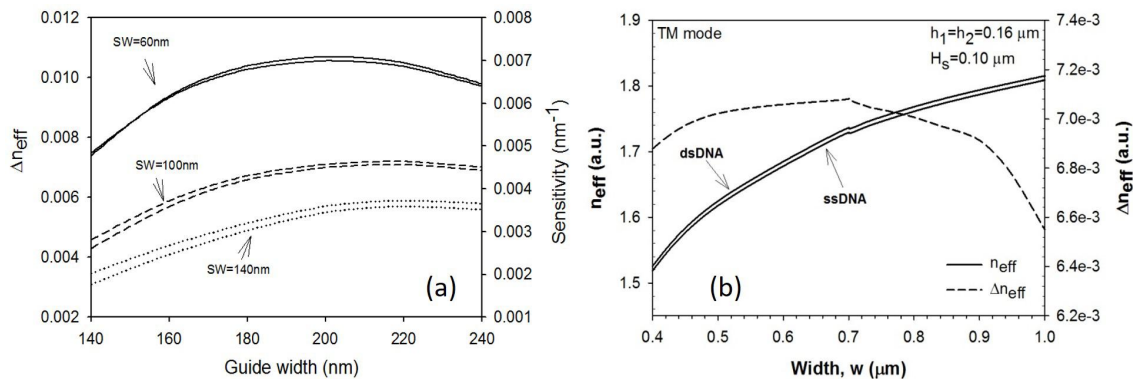


Figure 2. (a) Waveguide Δn_{eff} and sensitivity variations with Si core width for a vertical slot waveguide, (b) n_{eff} and Δn_{eff} variations with Si core width for horizontal slot waveguide.

3.2 SOI based cross-slot waveguide

In the previous section (Section 3.1), the vertical and horizontal slot guides can only guide the quasi-TE and TM modes, respectively i.e. they are highly polarization dependent. This difficulties could be resolved with a cross-slot waveguide. It is also useful for biochemical sensing which supports the much stronger field enhancement in the slot region for both quasi-TE and TM modes. The cross-slot design contains both vertical and horizontal slots simultaneously shown in Fig. 3(a). Figures 3(b) and (c) show the FV-FEM simulated E_x field profiles of quasi-TE and E_y field profile of quasi-TM modes, respectively. The ratio of the total slot confinement factors for the quasi-TE and TM modes ($\Gamma_{T-Hy}/\Gamma_{T-Hx}$) is an important parameter for optimization to make the device polarization independent. Figures 3(d) and (e) depict the variations of $\Gamma_{T-Hy}/\Gamma_{T-Hx}$ with the width (W) and height (H) of silicon cores, respectively. The ideal ratio of 1 is shown by the black dashed lines where the device shows its polarization independence.

The device is used for surface sensing.³ A bio-layer of thickness $t_{bio} = 5$ nm and refractive index of 1.45 is considered. It is obtained that the sensitivities for both polarization modes increase with the decrement of

Si core width or height. For the same cross-slot width and height of 100 nm, the sensitivity value for each polarization mode is 0.012 per nm, which is two times of vertical or horizontal slot waveguide sensitivity with similar dimensions. The sensitivities for both quasi-TE and TM modes can be improved by reducing the width and height of cross-slot simultaneously.

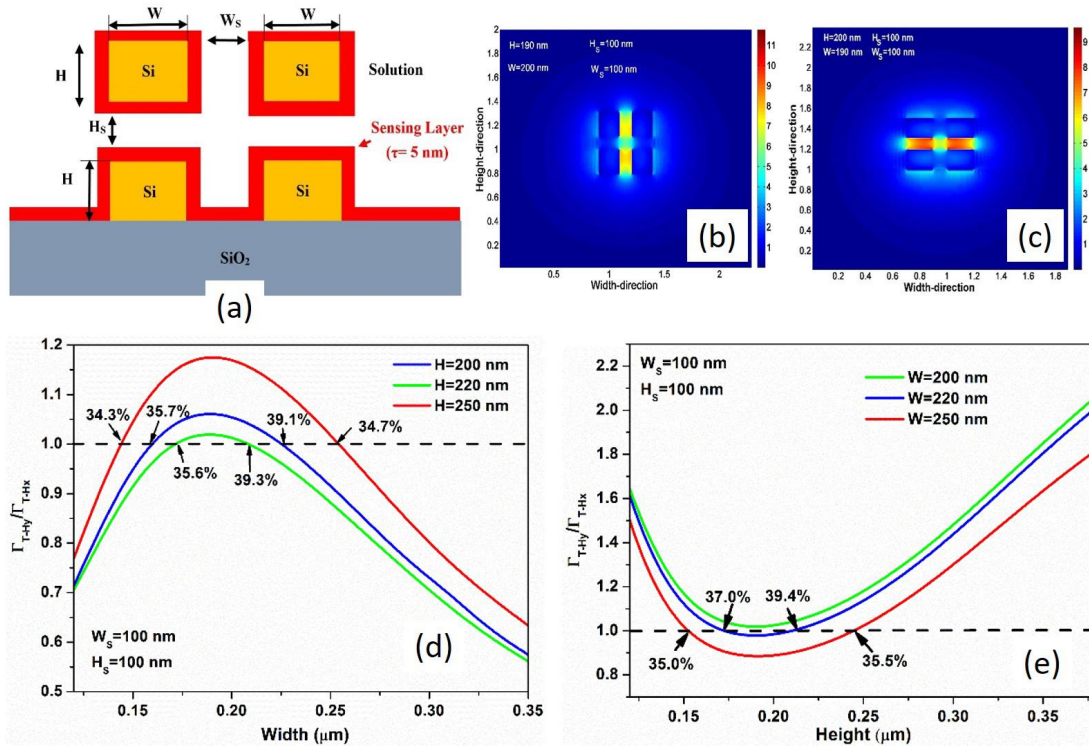


Figure 3. (a) Schematic cross-section of cross-slot waveguide, (b) and (c) are the FV-FEM simulated modal distributions, (d) and (e) show the ratio of quasi-TE and TM slot confinement with Si core width and height, respectively.

3.3 Hybrid plasmonic horizontal slot waveguide

The hybrid plasmonic slot waveguide is composed of lossy silver (Ag) layer, porous ZnO (P-ZnO), silicon (Si) and silica (SiO_2). The P-ZnO layer is sandwiched in between metal and high index Si, shown in Fig. 1.7.1(a). This novel waveguide structure guides the light through its low index slot region as a supermode that is a coupled form of the surface plasmon (SP) mode and dielectric waveguide mode. The SP mode is highly TM-polarized in nature and that can be excited either by electrons or photons having same frequency and momentum. This waveguide supports both quasi-TE and TM modes. However, the plasmonic supermode which is quasi-TM polarized is concentrated in the low index region, whereas, the quasi-TE mode is guided by the high index Si core. The porous ZnO (P-ZnO) is used as a low index medium which shows a comparative lower index than that of bulk ZnO, as the P-ZnO contains air filled pores. Figure 4(b) shows the power confinement variations of the fundamental quasi-TM and TE modes with slot thickness (t_{slot}) for three different core widths, $W_{\text{core}} = 350, 450,$ and 550 nm. For all three W_{core} s the quasi-TM power confinements ($\Gamma_{\text{TM-slot}}$), shown by solid lines, increase with t_{slot} increment, reach a maximum value of 41.79% at $t_{\text{slot}} = 70$ nm and then decrease gradually with further increment of t_{slot} . However, a $t_{\text{slot}} = 100$ nm shows a small power confinement variation than that of $t_{\text{slot}} = 70$ nm. Therefore, a 100 nm ZnO slot has been considered that makes the waveguide easy for fabrication. Figure 4(c) shows the quasi-TM and TE effective index difference ($\Delta Re(n_{\text{eff}})$) of with the absorbed ethanol volume fraction for different ZnO porous region of porosity of $P = 30\%, 40\%, 50\%,$ and 60% . The $\Delta Re(n_{\text{eff}})$ for the quasi-TM mode shows much higher response than that for the TE mode. This indicates that the hybrid plasmonic quasi-TM mode is more sensitive in compare to the quasi-TE mode. depict the waveguide TM modal

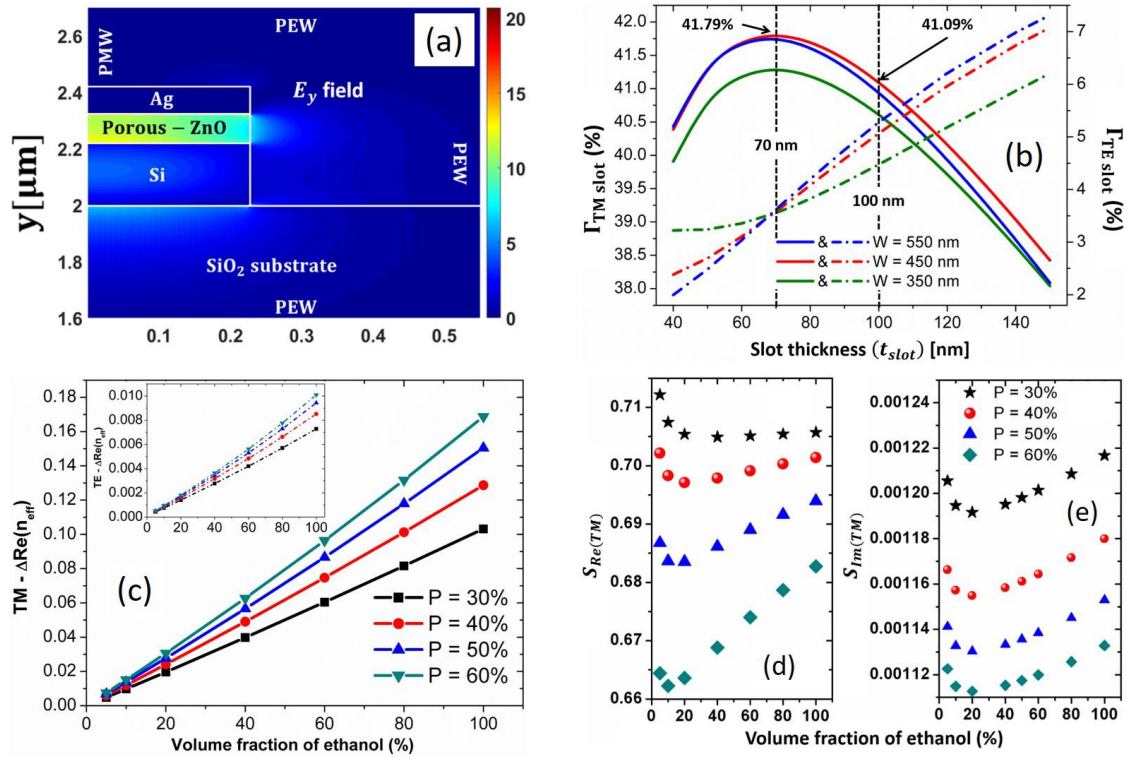


Figure 4. (a) FV-FEM simulated quasi-TM mode of hybrid plasmonic waveguide, (b) Quasi-TM and TE slot confinement with slot thickness (t_{slot}), (c) Effective index difference of quasi-TM and TE modes with different volume fraction of ethanol for fixed ZnO Porosity of 30%, 40%, 50%, and 60%. (d) waveguide sensitivity variation with ethanol vapour absorption.

sensitivity variations for both real and imaginary effective index.

The black, red, blue, and cyan markers in Fig. 4(d) depict the real effective index sensitivity ($S_{Re(TM)} = \Delta Re(n_{eff})/\Delta n_{slot}$) and normalized attenuation sensitivity ($\Delta Im(n_{eff})/\Delta n_{slot}$) of the fundamental quasi-TM mode for porosity, $P = 30\%$, 40% , 50% and 60% , respectively. The $S_{Re(TM)}$ and $S_{Im(TM)}$ initially decreases and then increases with the increase of volume fraction of absorbed ethanol. The sensitivity curves also indicate that the lower porosity ($P = 30\%$) ZnO layer shows sensitivity than that of the higher porosity ZnO. In case of waveguide based sensor, the real effective index based sensitivity change is more important than imaginary index based change, shown in Figs. 4(d) and (e). Here, our proposed waveguide shows a higher real effective index based sensitivity of 0.70 per RIU.

3.4 ZnO coated gold (Au) nanowire

Gold (Au) nanoparticles are of researcher's interest due to its plasmonic properties at visible wavelengths. In this section, an Au nanowire with an Al^{+3} doped ZnO (AZO) cladding layer has been designed and studied with our in-house FV-FEM for the application gas sensing. A small concentration of Al^{+3} doping in ZnO results in a replacement of Zn atoms by Al atoms which on the other way increase the conductivity of doped ZnO. As a practical device, a finite dimension AZO coated Au nanowire with height, $h = 60$ nm and width, $w = 250$ nm is considered, as shown in the inset of Fig. 5(a). A 100 nm AZO clad along with infinitely extent air clad is considered for computations. Figure 5(a) shows that the refractive index of AZO reduces from its undoped ZnO value with the increase of carrier concentrations (N) and therefore, the quasi-TM mode effective index decreases. Additionally, as N increases the material loss also increases due to increasing material conductivity. Therefore, for this waveguide both the change in effective index and differential loss could be considered for gas sensing investigations. The effective index difference and the differential loss can be expressed as

$$\Delta n_{eff} = |n_{eff}(N_L) - n_{eff}(N)| \quad (3)$$

and

$$\Delta Loss = |Loss(N_L) - Loss(N)| \text{ in dB/mm} \quad (4)$$

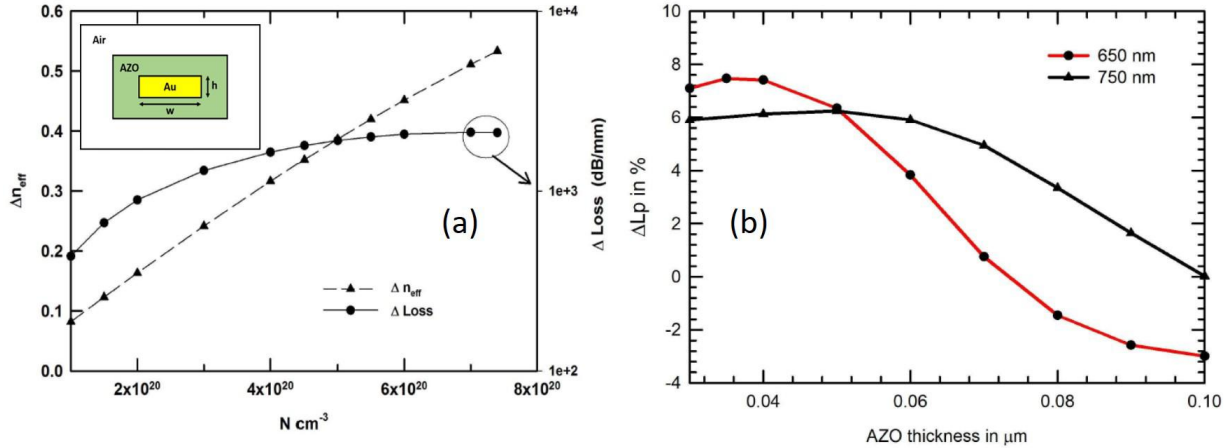


Figure 5. (a) effective index difference (Δn_{eff}) and loss difference ($\Delta Loss$) with the AZO cladding region at the operating wavelength of 750 nm. Inset shows the cross-section of the finite Au core AZO clad plasmonic waveguide of width 250 nm and height 60 nm. (b) Change in propagation length (ΔL_p) with AZO cladding layer thickness at two wavelengths of 650 and 759 nm.

Electrons are the majority charge carrier in the AZO layer. Therefore, absorption of any analyte such as gas, vapour, and liquid on the AZO surface will deplete electrons, resulting in a decrease in conductivity.

Figure 5(b) depicts the percentage change in propagation length (ΔL_p %) with the AZO layer thickness for two different wavelengths of 650 and 750 nm. The red ($\lambda = 650$ nm) and black ($\lambda = 750$ nm) lines in Fig. 5(b) depict that modal propagation length change (ΔL_p) increases from its negative and reaches maximum values in positive. For a larger thickness, the ΔL_p becomes negative whereas, for lower AZO thickness ΔL_p becomes positive. For a lower thickness of AZO cladding the power confinement in the depletion and metal core decrease. It is also notable that the close position of the depletion and metal core influences the surface plasmonic mode such that the modal loss increases with the increasing refractive index in the depletion layer. Therefore, any change in the surrounding external and in the AZO layer would affect the mode effective index and modal loss which can easily be detected from the light guiding property of the proposed waveguide.

3.5 SOI based slot resonator

Slot waveguide based photonic devices have attracted a lot of researcher's interest due to its unique light guiding property. Low index guiding enhance the the light-matter interaction which makes this waveguide useful for bio and chemical sensing applications. The effective use of slot waveguide based ring resonator suffers from the bending loss. This bending loss can be removed by considering a straight slot resonator instead of a bend one. Figure 6(a) depicts the schematic setup of the complete straight resonator section. The slotted resonator is a short length of straight vertically slotted waveguide. Thus, the cross-sectional design parameters can be optimized by 2-D FV-FEM. Generally, a SOI waveguides with height $H = 220$ nm is widely used, however, in our study a high power confinement can be achieved into slot with a higher core height. Therefore, the core height is taken as 500 nm for our device. Thus, with the optimized design parameters the device length (L) can be calculated as $2L = n\lambda_{res}/n_{eff}$. Here $2L$ denotes the round-trip length of the electromagnetic wave in the resonator. The device length is calculated as 473 nm for the expected resonating wavelength of 1550 nm for the fundamental longitudinal mode.

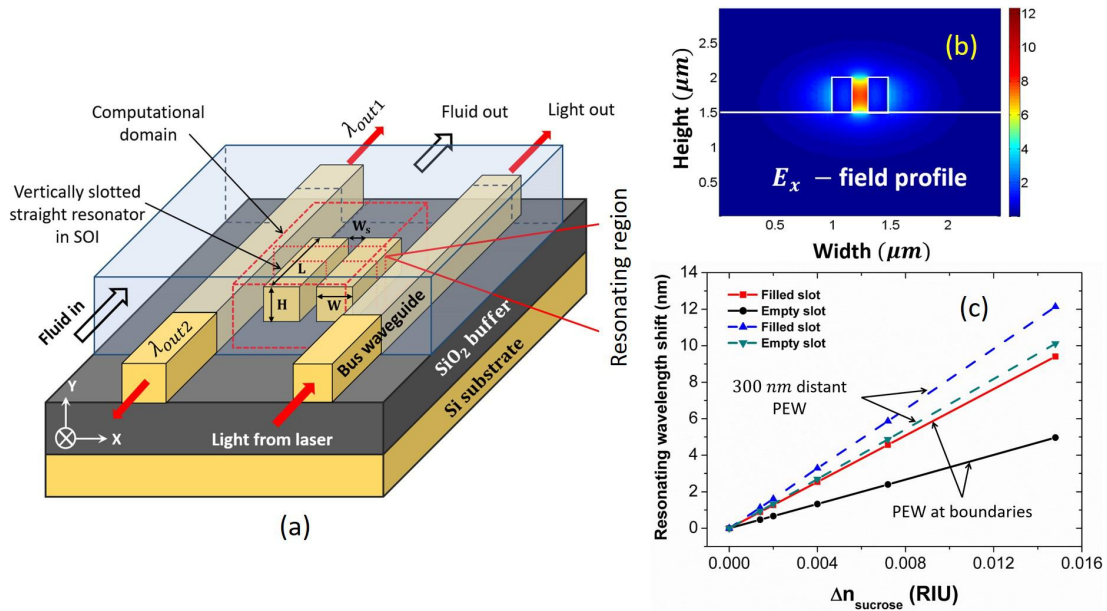


Figure 6. (a) 3-D schematic diagram of vertical slotted straight resonator, (b) FV-FEM simulated cross-sectional field distribution of the vertical slot, (c) Variation of the resonating wavelength shift with the refractive index change of the sucrose solution of different concentrations.

The bounded resonator field gets confined in the cavity and oscillates at a particular frequency into low index slot region. The resonating wavelength of the structure demands a complete 3-D analysis. Therefore, a dedicated 3-D FV-FEM code has been developed and used to analyze the device as a whole. The device response has been tested for both the bulk and surface sensing applications. Figure 6(c) shows the resonating wavelength shift of the straight resonator depending on the refractive index change in the sucrose solution. During bulk sensing process we also considered two different cases, (1) when the sensing liquid filled the slot completely and (2) when the slot is filled completely or partially by the air bubbles. The simulated results show a much higher bulk sensitivity of 635 nm/RIU and 335 nm/RIU for the filled and empty slot condition. Similarly, for surface sensing application we considered a 5 nm bio-layer of refractive index of 1.45 on top of Si and slot region. The device shows a 5.2 nm resonating wavelength shift due to the presence of the bio-layer.

4. CONCLUSION

In this article we presented several SOI and hybrid plasmonic based waveguides and resonators. All these devices were designed and optimized with our in-house numerically accurate full-vectorial finite element method (FV-FEM). For the waveguide modal field distributions we used our in-house 2-D FV-FEM code and for the three dimensional resonating devices 3-D FV-FEM code has been developed and used. Some selected results on recent developed high index contrast and hybrid plasmonic photonic devices were presented to show their usefulness in the field of bulk and surface sensing applications. Thus, this article presents a wide range of photonic waveguides and resonators which have great potentials in the field of photonic sensing devices.

ACKNOWLEDGMENTS

This work was supported by City, University of London, UK and in part by Erasmus Mundus AREAS+ Ph.D. fellowship program.

REFERENCES

- [1] Dar, T., Homola, J., Rahman, B. M. A., and Rajarajan, M., "Label-free slot-waveguide biosensor for the detection of DNA hybridization," *Applied optics* **51**(34), 8195–8202 (2012).

- [2] Viphavakit, C., Komodromos, M., Themistos, C., Mohammed, W. S., Kalli, K., and Rahman, B. M. A., "Optimization of a horizontal slot waveguide biosensor to detect DNA hybridization," *Applied optics* **54**(15), 4881–4888 (2015).
- [3] Pan, C. and Rahman, B. M. A., "High-sensitivity polarization-independent biochemical sensor based on silicon-on-insulator cross-slot waveguide," *IEEE Journal of Selected Topics in Quantum Electronics* **23**(2), 64–71 (2017).
- [4] Ghosh, S. and Rahman, B. M. A., "A compact Mach–Zehnder interferometer using composite plasmonic waveguide for ethanol vapor sensing," *Journal of Lightwave Technology* **35**(14), 3003–3011 (2017).
- [5] Aminah, N. S., Themistos, C., Hidayat, R., Djamal, M., Rahman, B., et al., "Evolution of surface plasmon supermodes in metal-clad microwire and its potential for biosensing," *Journal of Lightwave Technology* **35**(21), 4684–4691 (2017).
- [6] Kejalakshmy, N. T., Grattan, K. T. V., and Rahman, B. M. A., "Investigation of the optical modal properties of Al+ 3 doped ZnO-coated Au waveguide for gas sensing applications using the finite element method," *IEEE Sensors Journal* **16**(5), 1176–1181 (2015).
- [7] Ghosh, S. and Rahman, B. M. A., "An innovative straight resonator incorporating a vertical slot as an efficient bio-chemical sensor," *IEEE Journal of Selected Topics in Quantum Electronics* **23**(2), 132–139 (2017).
- [8] Berk, A., "Variational principles for electromagnetic resonators and waveguides," *IRE Transactions on Antennas and Propagation* **4**(2), 104–111 (1956).
- [9] Ghosh, S. and Rahman, B. M. A., "Evolution of plasmonic modes in a metal nano-wire studied by a modified finite element method," *Journal of Lightwave Technology* **36**(3), 809–818 (2018).
- [10] Ghosh, S. and Rahman, B. M. A., "Design of on-chip hybrid plasmonic Mach-Zehnder interferometer for temperature and concentration detection of chemical solution," *Sensors and Actuators B: Chemical* **279**, 490 – 502 (2019).